Journal of Vibration and Control
http://jvc.sagepub.com/

Effective Sensor Placements for the Estimation of Proper Orthogonal Decomposition Mode Coefficients in von Karman Vortex Street

Kelly Cohen, Stefan Siegel, Dave Wetlesen, Jeff Cameron and Aaron Sick

Journal of Vibration and Control 2004 10: 1857
DOI: 10.1177/1077546304046035

The online version of this article can be found at:
http://jvc.sagepub.com/content/10/12/1857

Published by:
SAGE
http://www.sagepublications.com

Effective Sensor Placements for the Estimation of Proper Orthogonal Decomposition Mode Coefficients in von Kármán Vortex Street

KELLY COHEN
STEFAN SIEGEL
DAVE WETLESEN
JEFF CAMERON
AARON SICK
HQ United States Air Force (USAF) Academy/DFAN, 2354 Fairchild Dr, Suite 6H27, USAF Academy, Colorado 80840, USA (YonaKelly1@aol.com)

(Received 18 September 2003; accepted 5 May 2004)

Abstract: For feedback control using low-dimensional proper orthogonal decomposition (POD) models, the mode amplitudes of the POD mode coefficients need to be estimated based on sensor readings. This paper is aimed at suppressing the von Kármán vortex street in the wake of a circular cylinder using a low-dimensional approach based on POD. We compare sensor placement methods based on the spatial distribution of the POD modes to arbitrary ad hoc methods. Flow field data were obtained from Navier–Stokes simulation as well as particle image velocimetry (PIV) measurements. A low-dimensional POD was applied to the snapshot ensembles from the experiment and simulation. Linear stochastic estimation was used to map the sensor readings of the velocity field on the POD mode coefficients. We studied 53 sensor placement configurations, 32 of which were based on POD eigenfunctions and the others using ad hoc methods. The effectiveness of the sensor configurations was investigated at Re = 100 for the computational fluid dynamic data, and for a Reynolds number range of 82–99 for the water tunnel PIV data. Results show that a five-sensor configuration can keep the root mean square estimation error, for the amplitudes of the first two modes to within 4% for simulation data and within 10% for the PIV data. This level of error is acceptable for a moderately robust controller. The POD-based design was found to be simpler, more effective, and robust compared to the ad hoc methods examined.

Key Words: Flow control, sensor placement and number, proper orthogonal decomposition, linear stochastic estimation

NOMENCLATURE

$a_n(t)$	time-dependent coefficient, of nth mode, of the low-dimensional model
b_n	coefficients associated with the control input, of nth mode, of low-dimensional model
C_s^n	coefficients of the linear stochastic estimator
C_d	mean drag coefficient $C_d = F_D/0.5\ \rho\ U_\infty{}^2\ 1\text{m}^2$
D	cylinder diameter
f	vortex shedding frequency

Journal of Vibration and Control, **10:** 1857–1880, 2004 DOI: 10.1177/1077546304046035

f_a	feedback control input to the cylinder
F_D	drag force
g_k	quadratic non-linear function used in low-dimensional, time-dependent model
Re	Reynolds number Re = $U_\infty D/\nu$
St	Strouhal number St = $f D/U_\infty$
u_s	sensor measurement of streamwise velocity
$\tilde{u}(x, y, t)$	velocity field
$U(x, y)$	mean flow
U_∞	freestream velocity
$u(x, y, t)$	fluctuating velocity component
x, y	spatial coordinates
α	skew angle of attack of the incoming flow used to introduce initial perturbation
$\Phi(x, y)$	spatial eigenfunction
ν	kinematic viscosity

1. INTRODUCTION

Many flows of engineering interest produce vortex shedding. A textbook example of vortex shedding behind a circular cylinder has been a subject of extensive research for almost a century. Applications concerning aircraft and missile aerodynamics include dynamic stall control and lift enhancement (Gillies, 1998). Additional applications are found in the field of chemical mixing improvement, marine structures, submarine periscopes, and civil and wind engineering (von Kármán, 1954). The ability to control the wake of a bluff body could be used to reduce drag (Ahlorn et al., 2002), increase mixing and heat transfer, and enhance combustion (Park et al., 1993).

Shedding of counter-rotating vortices is observed in the wake of a two-dimensional cylinder above a critical Reynolds number (Re $\sim$ 47, non-dimensionalized with respect to freestream speed and cylinder diameter). This phenomenon is often referred to as the von Kármán vortex street (von Kármán, 1954). Figure 1, a photograph taken at the center line of an unforced cylinder wake at the USAF Academy's water tunnel, shows the von Kármán vortex street at Re = 120.

These flow-induced non-linear oscillations lead to some undesirable effects associated with unsteady pressures, such as fluid–structure interactions (Park et al., 1993) and lift/drag fluctuations (Roussopoulos, 1993). Also, the vortices themselves greatly increase the drag of the bluff body, when compared to the steady wake that can be observed at lower Reynolds numbers.

For these reasons, many attempts to improve the unsteady vortex street have been made. When active open-loop forcing of the wake is used, the vortices in the wake can be locked in phase to the forcing signal. This also strengthens the vortices and, consequently, increases the drag. The cylinder wake may be controlled by forcing the flow, and several different forcing techniques affect the behavior of the flow. However, the wake response is similar for different types of forcing. The following forcing methods have been used: acoustic excitation of the wake, longitudinal, lateral or rotational vibration of the cylinder, and alternate blowing

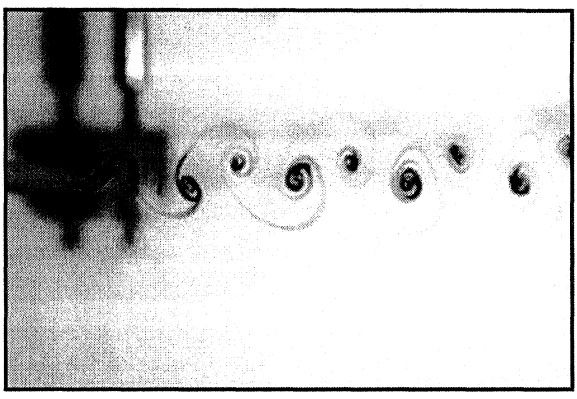

Figure 1. Unforced wake of circular cylinder (Re = 120, diameter D = 3.97 mm, U_∞ = 30 mm s^{-1}.)

and suction at separation points (Blevins, 1990). An effective way of suppressing the self-excited flow oscillations, without making changes to the geometry, is by the incorporation of active closed-loop flow control (Gillies, 1998).

A closed-loop flow control system is comprised of an actuator (or set of actuators) that introduces a perturbation into the flow, to obtain desired performance. Furthermore, the controller acts upon information provided by a set of sensors. The basic closed-loop control strategies are the model-independent approach, the optimal/suboptimal control approach, and the low-dimensional approach.

1.1. Model-Independent Approach

This involves the introduction of sensors in the wake and a control law (usually linear) which produces a command to the actuator that forces the flow. The advantages of this approach (Roussopoulos, 1993) are:

- no model of the flow field is required for controller design;
- direct feedback eliminates the need for a state estimator;
- a simple control law may be implemented in an experimental setup with relative ease.

Experimental studies show that a linear proportional feedback control based on a single sensor feedback is able to delay the onset of the wake instability, rendering the wake stable at Re about 20% higher than the unforced case. Above Re = 60, a single-sensor feedback may suppress the original mode but destabilizes one of the other modes. This approach is relatively simple to implement experimentally. However, the results are of limited use for the challenging problem of an absolutely unstable wake.

1.2. Optimal/Suboptimal Control Approach

This approach is more structured as it applies conventional and proven model-based control strategies such as optimal control theory for flow control problems. The central idea

here is to minimize a cost function that satisfies the Navier–Stokes equations that govern the flow. For example, Abergel and Temam (1990) developed conditions for optimality, which minimizes a cost function that represents the drag on a body. The main disadvantage of the optimal control approach is the computational problems associated with the non-linearities of the cumbersome unsteady Navier–Stokes equations. To illustrate this issue, Li et al. (2003) point out that for a steady-state problem that has N time-steps, the dimension of the unsteady problem is N times larger in comparison. This drawback adversely affects real-time implementation of optimal flow control and has led to the development of several suboptimal approaches surveyed by Li et al. (2003).

1.3. Low-Dimensional Approach

Low-dimensional modeling is a vital building block when it comes to realizing a structured model-based closed-loop strategy for flow control. For control purposes, a practical procedure is needed to break down the velocity field, governed by Navier–Stokes partial differential equations, by separating space and time. A common method used to substantially reduce the order of the model is proper orthogonal decomposition (POD) (Holmes et al., 1996). This method is an optimal approach in that it requires the lowest amount of modes to attain a given energy residual. The POD method may be used to identify the characteristic features, or modes, of a cylinder wake as demonstrated by Gillies (1998).

Low-dimensional modeling, based on POD techniques, is a vital building block when it comes to realizing a structured model-based closed-loop strategy for flow control. The POD procedure decomposes the velocity field into spatial eigenfunctions and temporal mode amplitudes.

The major building blocks of this structured approach are comprised of a reduced-order POD model, a state estimator, and a controller. The desired POD model contains an adequate number of modes to enable accurate modeling of the temporal and spatial characteristics of the large-scale coherent structures inherent in the flow. Further details of the POD method may be found in Holmes et al. (1996). A common approach, referred to as the method of "snapshots" introduced by Sirovich (1987), is used to generate the basis functions of the POD spatial modes from flow field information obtained using either experiments or numerical simulations. This approach to modeling the global behavior of the wake behind a circular cylinder was used by Gillies (1998), and is also the approach followed in this paper.

For low-dimensional control schemes to be implemented, a real-time estimation of the modes present in the wake is necessary, since it is not possible to measure them directly. Figure 2 presents a schematic illustration of the various blocks within the low-dimensional approach. The controller acts on the flow (not shown in the figure). POD mode coefficient estimation is provided by implementing linear stochastic estimation (LSE). The time histories of the temporal coefficients of the POD model are determined by applying least-squares fitting to the spatial eigenfunctions and the snapshots of the flow. Sensor measurements may take the form of wake velocity measurements, as in this paper, or body-mounted pressure measurements.

The requirement for the estimation scheme then is to act as a modal filter that separates the modes. The main aim of this approach is to prevent the destabilizing effects of observation spillover as described by Balas (1978). Spillover has been the cause for instability in

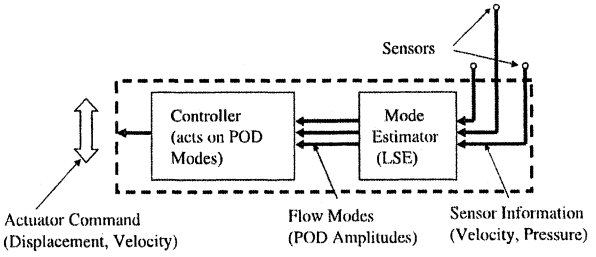

Figure 2. Low-dimensional control strategy.

the control of flexible structures, and modal filtering was found to be an effective remedy (Meirovitch, 1990). The intention of the proposed strategy is that the signals, provided by a certain configuration of sensors placed in the wake, are processed by the estimator to provide the estimates of the first two modes. The estimation scheme, based on the LSE procedure introduced by Adrian (1977), predicts the temporal amplitudes of the POD modes from a finite set of measurements obtained from either computational or experimental data. The LSE of POD modes was successfully implemented by Cohen et al (2003b) for control of the Ginzburg–Landau wake model. A major design challenge lies in finding an appropriate number of sensors and their locations that will enable the desired modal filtering. The need for modal filtering and the search for suitable sensor configurations is a problem common to the control of flexible structures, where a considerable amount of work has been carried out (Baruh and Choe, 1990; Lim, 1997) and can be leveraged. Meirovitch (1990) provides a survey of some effective strategies.

In the next section we describe the research objective and the uniqueness of the developed approach. The Navier–Stokes, computational fluid dynamic (CFD) model is described and presented in the following section, and the development of the low-dimensional POD model is described subsequently. Then, based on the POD model, 32 different sensor configurations are developed and their effectiveness is tested with CFD data. The POD-based sensor configurations are compared to 19 ad hoc designs. The next section describes the experimental setup. This is followed by the development of a lookup table aimed at providing gain-scheduling estimation of the low-dimensional states as the Reynolds number is varied. The final section summarizes the conclusions of this research and provides recommendations for future work.

2. RESEARCH OBJECTIVE

Past research on the closed-loop flow control of a cylinder wake incorporates sensor configurations based on an ad hoc approach obtained by trial and error methods. The main objective of this paper is to develop, demonstrate, and experimentally validate a more generic approach to determining the sensor number and location for real-time estimation of the truncated POD states of a cylinder wake. To the best of our knowledge, this represents the first time POD modeling has been used as a basis for selection of sensor number and placement. It will

be shown that effective sensor configurations may be based on the spatial distributions of a low-dimensional POD model. The robustness of these sensor configurations to perturbations in the Reynolds number will be examined.

3. COMPUTATIONAL MODEL

In order to obtained two-dimensional unsteady data of the cylinder wake, a CFD simulation was performed. The model primarily needs to accurately capture the dynamic behavior of the flow field, and this need to be verified with experimental data presented in literature. We used COBALT, a CFD solver with the following parameters (see Cobalt Solutions, LLC, http://www.cobaltcfd.com):

- two-dimensional cylinder, diameter = 1 m;
- Reynolds number (Re) = 100;
- laminar Navier–Stokes equations;
- spatial and temporal second-order accuracy;
- mean flow, $U = 34$ m s^{-1};
- damping coefficients, advection = 0.01 and diffusion = 0.00;
- 32 iterations for matrix solution scheme;
- three Newtonian subiterations;
- non-dimensional time-step, $\Delta t = 0.05$;
- time-step, $\Delta t = 0.00147$ s.

The simulation was triggered by skewing the incoming mean flow by $\alpha = 0.5°$ to introduce an initial perturbation. An important issue concerning the validity of the CFD model needs to be addressed before using the data. For validation of the unforced cylinder wake CFD model at Re = 100, the resulting value of the mean drag coefficient, C_d, will be compared to experimental and computational investigations reported in the literature. At Re = 100, experimental data, reported by Oertel (1990) and Panton (1996), point to C_d values from 1.26 to 1.4. Furthermore, Min and Choi (1999) report on several numerical studies that obtained drag coefficients of 1.35 and 1.337. The CFD model used in this paper results in C_d =1.35 at Re = 100, which compares well with the reported literature. Another important benchmark parameter concerns the value of the non-dimensional Strouhal number (St) for the unforced cylinder wake. Experimental results at Re = 100, presented by Williamson (1996), point to St values ranging from 0.163 and 0.166. The CFD model used in this paper has St = 0.163 at Re = 100, which compares well with the reported literature.

4. POD MODELING

POD, a non-linear model reduction approach, is also referred to in the literature as the Karhunen–Loeve expansion (Holmes et al., 1996). The desired POD model contains an adequate number of modes to enable modeling of the temporal and spatial characteristics of the large-scale coherent structures inherent in the flow.

Table 1. Energy content (eigenvalues) for the first eight modes of the POD model.

Mode I	Mode II	Mode III	Mode IV	Mode V	Mode VI	Mode VII	Mode VIII
52.54%	41.05%	2.90%	2.63%	0.39%	0.38%	0.05%	0.04%

In this paper, the method of "snapshots" introduced by Sirovich (1987) is used to generate the basis functions of the POD spatial modes from the numerical solution of the Navier–Stokes equations obtained using the CFD simulation. In all, 70 snapshots were used equally spaced at 0.00735 s apart. The time between snapshots is five times the simulation time-step. The snapshots were taken after ensuring that the cylinder wake flow reaching a steady-state limit cycle. Only the U velocity component (in the direction of the mean flow) was used for the sensor placement and number studies reported in this paper. For control design purposes, the POD method enables the Navier–Stokes equations to be modeled as a set of ordinary differential equations (ODEs).

The accurate POD construction was first described in the pioneering Galerkin modeling paper of Deane et al. (1991). The procedure has been generalized for transients by Gerhard et al. (2003). The POD algorithms, detailed in Cohen et al (2003b), based on the above steps, were applied to the CFD data obtained at Re = 100. The energy content for the first eight modes is presented in Table 1. It can be seen that more than 99.98% of the kinetic energy of the flow lies in the first eight modes. An important aspect of reduced-order modeling concerns truncation, i.e. answers to the following questions: how many modes are important and what are the criteria for effective truncation?

The answers to the above questions have been addressed by Cohen et al. (2003a), who have shown that control of the POD model of the von Kármán vortex street in the wake of a circular cylinder at Re = 100 is enabled using just the first mode. Furthermore, feedback based on the first mode alone suppressed all the other modes in the four-mode POD model. In view of this result, truncation of the POD model will take place after the first two modes, which contain more than 93.5% of the total amount of energy. At this point, it is imperative to note the difference between the number of modes required to reconstruct the flow and the number of modes required to control the flow. In this paper, we are interested in estimating only those modes required for closed-loop control. On the other hand, an accurate reconstruction of the velocity field based on a low-dimensional model may be obtained using between four and eight modes (Smith et al., 2002). The POD algorithm was applied to the velocity component in the direction of the flow as described in equation (1). The decomposition of this component of the velocity field is

$$\tilde{u}(x, y, t) = U(x, y) + u(x, y, t) \tag{1}$$

where U (m s^{-1}) denotes the mean flow. u (m s^{-1}) is the fluctuating component that may be expanded as

$$u(x, y, t) = \sum_{k=1}^{n} a_k(t)\phi_i^{(k)}(x, y) \tag{2}$$

where $\phi(x, y)$ represents the non-dimensional spatial eigenfunctions (see Figure 3) and $a_k(t)$ denotes the time-dependent coefficients having units of m s^{-1} (see Figure 4) determined from the POD procedure. For an arbitrarily forced circular cylinder, we can write the low-dimensional wake model as first suggested by Gillies (1998) as

$$\frac{da_k}{dt} = g_k(a_n) + b_k f_a \tag{3}$$

where g_k, for k modes, is a quadratic non-linear function of the time-dependent mode coefficients, b_k are coefficients associated with the control input, and f_a is the feedback control input to the cylinder. For the open-loop case $f_a = 0$. For a full-state feedback system, the closed-loop control input, f_a, is a function of a_k. However, it is not possible to obtain a direct measurement of a_k. The velocity field may be obtained from a CFD simulation or from a real-time particle image velocimetry (PIV) system as described by Siegel et al. (2003). The quintessential question is whether an effective estimate of the states, of the low-dimensional model, a_k, can be estimated based on the real-time velocity field. The answer is in the affirmative and the details of the procedures that provide the estimate of the first two modes, a_1 and a_2, are presented in the next section.

5. ESTIMATION

The time histories of the temporal coefficients of the POD model are determined by applying the least-squares technique to the spatial modes and the unforced flow. The intention of the proposed strategy is that the velocity measurements provided by the sensors are processed by the estimator to provide the estimates of the first two temporal modes. The estimation scheme, based on the LSE procedure introduced by Adrian (1977), predicts the temporal amplitudes of the first two POD modes from a finite set of velocity measurements obtained from the CFD solution of the uncontrolled cylinder wake. Further details of stochastic estimation of POD modes are provided by Bonnet et al. (1994). Recently, this method was also used by Carlson and Miller (2002) to predict the degree of flow separation from POD modes on a backward facing ramp using ramp pressure measurements.

For each sensor configuration, 70 velocity measurements were used equally spaced at 0.00735 s apart. All the measurements were taken after ensuring that the cylinder wake reached steady state. Only data concerning velocity component in the direction of the flow were used for the sensor placement and number studies reported in this paper. The temporal mode amplitudes, a_1 and a_2, presented in Figure 4 at the above 70 discrete times, were mapped onto the extracted sensor signals, u_s, as follows

$$a_n(t) = \sum_{s=1}^{m} C_s^n u_s(t) \tag{4}$$

where m is the number of sensors and C_s^n represents the coefficients of the linear mapping. The effectiveness of a linear mapping between for velocity measurements and POD states has been experimentally validated by Siegel et al. (2002). The coefficients C_s^n ($n = 1, 2; s =$

$1, m$) in equation (4) are obtained via the LSE method from the set of 70 discrete sensor signals and temporal mode amplitudes. For each sensor configuration, the effectiveness of the LSE process for the estimation of the first two temporal mode amplitudes, a_1 and a_2, is presented in Tables 2(a) and 2(b).

6. SENSOR CONFIGURATION

Closed-loop flow control is a relatively new research field and the issue of sensor placement and number has been dealt with in an ad hoc manner. In this paper, an attempt will be made to emulate some of the proven successes from the field of structural control. Heuristically speaking, when some very fine dust particles are placed on a flexible plate, excited at one of its natural frequencies, after a short while the particles arrange themselves in a certain pattern typical of those frequencies. The particles will be concentrated in the areas that do not experience any motion (the nodes). On the other hand, the areas where the motion is most active (the internodes) will be clean of particles. It is at the internodes that the vibrational energy of that particular mode is at a maximum, and sensors placed at these locations are extremely effective at estimating that particular mode.

The above heuristic approach has been used by de Noyer (1999) for locating effective sensor locations for acceleration feedback control, in order to alleviate tail buffeting of a high-performance twin-tail aircraft. Note the use of the term "effective sensor configuration" as it is based on validated heuristics as opposed to "optimal sensor configuration", which results from a mathematical pattern search for a sensor configuration. So, what needs to be done to determine an effective sensor configuration is to find the areas of energetic modal activity. The spatial eigenfunctions obtained from the POD procedure provide information concerning the location of areas where modal activity is at its highest. In Figure 3, these energetic areas would be the maxima (red) and minima (blue). Placing sensors at the energetic maxima and minima of each mode is the basic hypothesis of this paper, and the purpose of the CFD simulation is to design a sensor configuration, which is later validated using water-tunnel experiments. The respective sensor number and location of each configuration is presented in Tables 2(a) and 2(b). 53 sensor configurations were developed comprising 2, 3, 4, 5, 6, 8, and 10 sensors. The locations of the sensors in Tables 2(a) and 2(b) are referenced in terms of the coordinates, non-dimensionalized with respect to the cylinder diameter D, namely, X/D and Y/D. For ease of understanding, the locations of maxima or minima of mode 1 or mode 2 at a given position away from the cylinder are abbreviated as per the legend at the top of Table 2(a). The other coordinates are locations of sensors that overlap on the "hillsides" of maxima and minima of both modes. Configurations 1–12 explore sensor placement solely at the maxima/minima of the first two modes. Configurations 13–25 explore some maxima and minima and locations that overlap hillsides of maxima and minima. Configurations 26–32 explore solely overlapping hillside locations with priority for placement given to areas of higher mode 1 intensity.

21 ad hoc sensor configurations were developed based on column configurations placed progressively further downstream from the cylinder, row configurations placed from above the flow to abeam the cylinder to below the cylinder and arc configurations placed at increasing radii from the cylinder center.

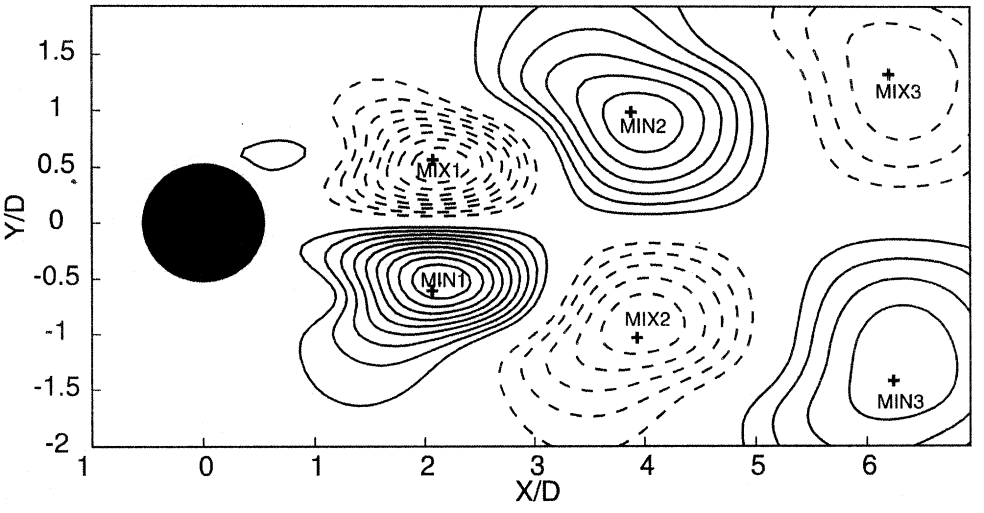

(a)

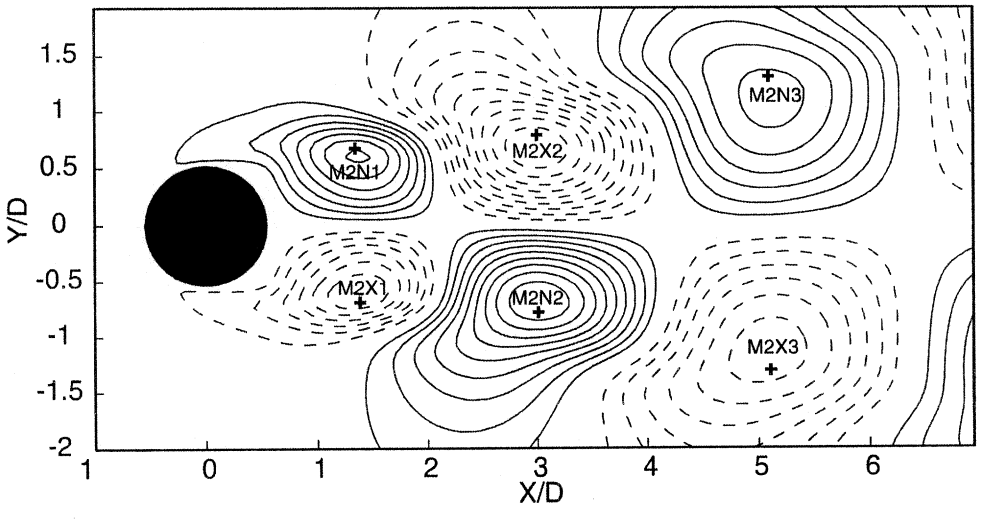

(b)

Figure 3. Spatial eigenfunctions, $\phi(x,y)$, of the POD model (CFD data): (a) mode 1; (b) mode 2.

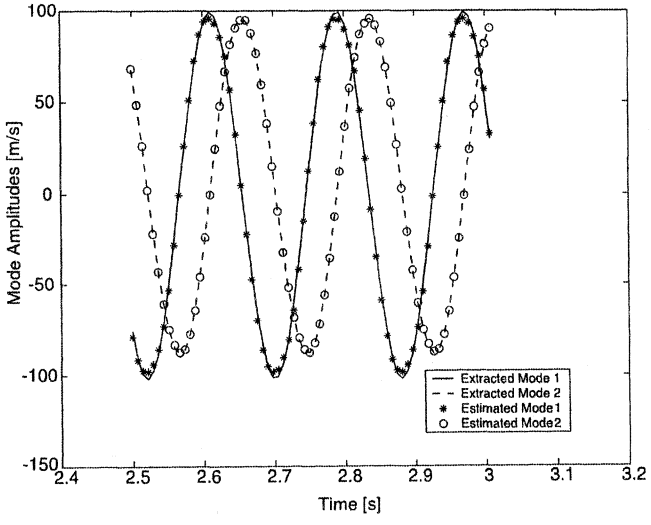

Figure 4. Estimated mode amplitudes projected on the desired (extracted) amplitudes for configuration 5 (CFD data).

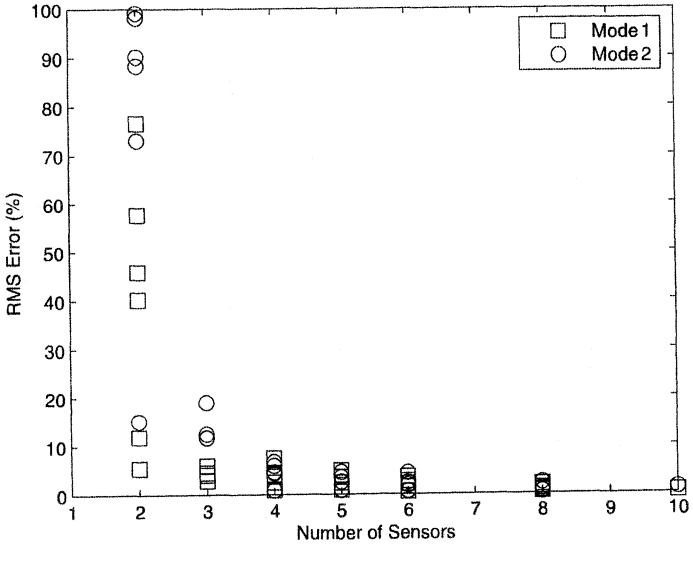

Figure 5. Estimation error versus number of sensors (CFD data at Re = 100), first 32 configurations.

Table 2(a). Estimation errors for sensor configurations at Re = 100 (CFD simulations) and Re = 99 (experiments) for the first 32 configurations.

Configuration no.	Sensors	Sensor coordinates (X/D, Y/D) M1/2=mode number X=maxima, N=minima Final number=position away from cylinder Example: M1X1=mode 1 first maxima (see Figure 3)	CFD Re=100 mode 1 error (%)	CFD Re=100 mode 2 error (%)	Exp. Re = 99 mode 1 error (%)	Exp. Re = 99 mode 2 error (%)
Sensors placed solely at maxima and minima						
1	2	M1X1=(2.2, 0.5), M1N1=(2.2, –0.5)	11.9	99.2	47	11
2	2	M1X1, M2N1=(1.4, 0.6)	57.7	73.0	63.0	10.9
3	3	M1X1, M1N1, M2N1	4.0	12.5	30	7
4	3	M1X1, M1N1, M2X2=(3.0, 0.7)	4.5	19.0	19.7	4.7
5	4	M1X1, M1N1, M2X1=(1.4,–0.6), M2N1	3.7	0.9	14	6
6	4	M1X1, M1N1, M2X2, M2N2=(3.0, –0.7)	4.1	4.4	14.5	3.8
7	4	M1N1, M1X2=(4, –1), M2X1, M2N2	7.5	6.7	14.5	2.9
8	5	M1X1, M1N1, M2X1, M2N1, M1N2=(4.0, 1)	3.5	0.8	10	5
9	5	M1N1, M1X2, M2X1, M2N2, M1N3	4.9	2.5	5.5	2.9
10	6	M1N1, M1X2, M2X1, M2N2, M1N3, M2X3	2.6	1.8	5.5	2.4
11	6	M1X1, M1N1, M2X1, M2N1, M1X2, M1N2	3.5	0.6	8	5
12	8	M1X1, M1N1, M2X1, M2N1, M1X2, M1N2, M2X2, M2N2	1.1	0.4	8	3
Maxima/minima and overlapping "hillsides"						
13	2	M1X1, (1.8, 0.5)	76.6	15.1	65	17
14	2	M1X1, (1.8, 0.75)	40.2	90.2	42	17
15	2	M1X1, (1.8, –0.75)	5.4	98.2	36	14
16	3	M1X1, (2.2, –0.75), M2N1	2.8	11.8	27	7
17	4	M1X1, (2.2, –0.75), M2N1, (1.4, –0.75)	2.5	5.9	12	4
18	5	M1X1, (2.2, –0.75), M2N1, (1.4, –0.75), (1.7, 0.30)	2.4	3.5	12	4
19	5	M1X1, M1N1, M2X1, M2N1, (3.5, 1) (overlaps hillsides of M1X2/M2N2)	3.5	0.9	10	5
20	6	M1X1, M1N1, M2X1, M2N1, (3.5, 1), (3.5, –1)	1.4	0.5	8	5
21	6	M1X1, (2.2, –0.75), M2N1, (1.4, –0.75), (1.7, 0.30), (1.5, –0.20)	2.1	2.4	12	4
22	8	M1X1, M1N1, M2X1, M2N1, (3.5, 1), (3.5, –1), (1.2, 1.0), (1.2, –1.0)	1.2	0.5	9	4
23	8	M1X1, M1N1, M2X1, M2N1, M2X2, M2N2, (3.5, 1), (3.5, –1)	0.8	0.4	8	3
24	8	M1X1, M1N1, M2X1, M2N1, (3.5, 1), (3.5, –1), (2.5, 1.5), (2.5, –1.5)	0.8	0.4	7	3
25	8	M1X1, (2.2, –0.75), M2N1, (1.4, –0.75), (1.7, 0.3), (1.5, –0.20), (0.65, 0.7), (2.0, –0.15)	1.9	1.1	12	3

Table 2(a). Continued.

Configuration no.	Sensors	Sensor coordinates (X/D, Y/D) M1/2=mode number X=maxima, N=minima Final number=position away from cylinder Example: M1X1=mode 1 first maxima (see Figure 3)	CFD Re=100 mode 1 error (%)	CFD Re=100 mode 2 error (%)	Exp. Re = 99 mode 1 error (%)	Exp. Re = 99 mode 2 error (%)
Overlapping hillsides with priority to mode 1						
26	2	(1.75, 0.5), (1.75, –0.5)	45.8	88.3	35	14
27	3	(1.75, 0.5), (1.75, –0.5), (2.4, 0.55)	6.0	11.7	34	9
28	4	(1.75, 0.5), (1.75, –0.5), (2.4, 0.55), (2.4, –0.55)	0.9	4.6	25	6
29	5	(1.75, 0.5), (1.75, –0.5), (2.4, 0.55), (2.4, –0.55), (3.7, 0.8)	0.9	4.5	16	5
30	6	(1.75, 0.5), (1.75, –0.5), (2.4, 0.55), (2.4, –0.55), (3.7, 0.8), (3.7, –0.8)	0.5	4.3	11	5
31	8	(1.75, 0.5), (1.75, –0.5), (2.4, 0.55), (2.4, –0.55), (3.7, 0.8), (3.7, –0.8), (4.6, 1.0), (4.6, –1.0)	0.5	2.3	9	2
32	10	(1.75, 0.5), (1.75, –0.5), (2.4, 0.55), (2.4, –0.55), (3.7, 0.8), (3.7, –0.8), (4.6, 1.0), (4.6, –1.0), (5.6, 1.15), (5.6, –1.15)	0.4	1.1	5	2

On the basis of a criterion associated with estimation accuracy, a certain configuration can either be given the "thumbs up" or not. The criterion selected to quantitatively examine the effectiveness of the sensor configuration is based on the root mean square (rms) of the error between the estimated and the extracted mode amplitudes. The extracted mode amplitudes are obtained by introducing the spatial eigenfunctions into the snapshot data of the velocity field using the least-squares method. For sake of convenience, this rms error is normalized with the rms of the desired extracted mode amplitudes, presented as a percentage. The resulting error percentage and the number of sensors may be integrated together into a cost function, and the purpose of the design process would then be to select the configuration that minimizes the cost. In this paper, we attempt to provide the necessary insight into possible trade-offs that need to be determined depending on the specific application. The above procedure is worked out individually for each of the two modes. The resulting sensor performance is presented in Tables 2(a) and 2(b). In this section we concentrate on the two columns that present the results based on CFD simulation data. A typical estimated versus desired mode amplitude plot, for sensor configuration 5, is presented in Figure 4. For this configuration, the rms estimation errors (from Table 2(a)) are 3.7% and 0.9% for modes 1 and 2, respectively.

Close examination of the performance comparison table provides an insight into the importance of having a quantitative criterion. Compared to configuration 1, configuration 3 provides a relatively better estimation for mode 2. However, the mode 1 error may not be acceptable. How much is acceptable? This would depend on the demands of the control system. Typically, as the number of sensors is increased, the error is reduced, as seen in Figure 5. Table 2(a) shows that for most of the six, eight, and ten sensor configurations, the error is two orders of magnitude lower than the desired signal. This clearly represents an

Table 2(b). Estimation errors for 21 ad hoc sensor configurations at Re = 100 (CFD simulations) and Re = 99 (experiments).

Configurations		CFD data		Experimental data	
		Mode 1 error	Mode 2 error	Mode 1 error	Mode 2 error
Columns					
33	(0.5,1)(0.5,0.5)(0.5,0)(0.5,–0.5)(0.5,–1) **C1**	1.3	0.7	58.2	5.8
34	(1,1)(1,0.5)(1,0)(1,–0.5)(1,–1) C2	0.8	0.9	33.6	12.0
35	(1.5,1)(1.5,0.5)(1.5,0)(1.5,–0.5)(1.5,–1) **C3**	1.6	3.2	18.4	12.9
36	(2,1)(2,0.5)(2,0)(2,–0.5)(2,–1) **C4**	1.7	5.7	34.7	8.1
37	(2.5,1)(2.5,0.5)(2.5,0)(2.5,–0.5)(2.5,–1) **C5**	9.4	5.8	39.6	3.8
38	(3,1)(3,0.5)(3,0)(3,–0.5)(3,–1) **C6**	23.4	4.0	41.1	4.9
39	(3.5,1)(3.5,0.5)(3.5,0)(3.5,–0.5)(3.5,–1) **C7**	26.7	28.1	27.4	8.5
40	(4,1)(4,0.5)(4,0)(4,–0.5)(4,–1) **C8**	7.4	53.6	13.2	7.7
Rows					
41	(1,1.5)(1.5,1.5)(2,1.5)(2.5,1.5)(3,1.5) **R1**	6.3	1.9	8.5	2.8
42	(1,1)(1.5,1)(2,1)(2.5,1)(3,1) **R2**	4.9	3.9	11.2	3.1
43	(1,0.5)(1.5,0.5)(2,0.5)(2.5,0.5)(3,0.5) **R3**	7.6	5.6	42.0	7.7
44	(1,0)(1.5,0)(2,0)(2.5,0)(3,0) **R4**	99.6	98.4	46.5	13.7
45	(1,–0.5)(1.5,–0.5)(2,–0.5)(2.5,–0.5)(3,–0.5) **R5**	7.9	5.9	15.3	7.1
46	(1,–1)(1.5,–1)(2,–1)(2.5,–1)(3,–1) **R6**	4.6	4.5	11.1	3.2
47	(1,–1.5)(1.5,–1.5)(2,–1.5)(2.5,–1.5)(3,–1.5) **R7**	6.4	2.4	9.0	2.9
Arcs					
48	(0.866, 0.5) (0.966, 0.26) (1, 0) (0.966, –0.26) (0.866, –0.5) **A1**	3.3	0.6	44.5	14.0
49	(1.3, 0.75) (1.45, 0.39) (1.5, 0) (1.45, –0.39) (1.3, –0.75) **A2**	8.2	4.6	13.5	13.7
50	(1.73, 1) (1.93, 0.52) (2, 0) (1.93, –0.52) (1.73, –1) **A3**	0.8	4.8	15.4	8.1
51	(2.17, 1.25) (2.41, 0.65) (2.5, 0) (2.41, –0.65) (2.17, –1.25) **A4**	3.0	1.4	31.3	6.7
52	(2.6,1.5) (2.9, 0.776) (3,0) (2.9, –0.776) (2.6,–1.5) **A5**	1.7	1.4	26.1	3.5
53	(3, 1.75) (3.4, 0.91) (3.5, 0) (3.4, –0.91) (3, –1.75) **A6**	5.1	10.1	25.8	4.4

acceptable signal-to-error ratio. For some applications as few as four or five sensors may be acceptable.

The results in Table 2(a) show that giving priority to the maxima and minima of the spatial eigenfunctions closest to the cylinder yields less error than priority given to the maxima and minima with the greatest intensity (configuration 5 versus configuration 6). However, configuration 6 yields a balanced error. Configurations 26–32 employ a heuristic focusing on overlapping intensities between modes 1 and 2 with a preference given to the intensity of

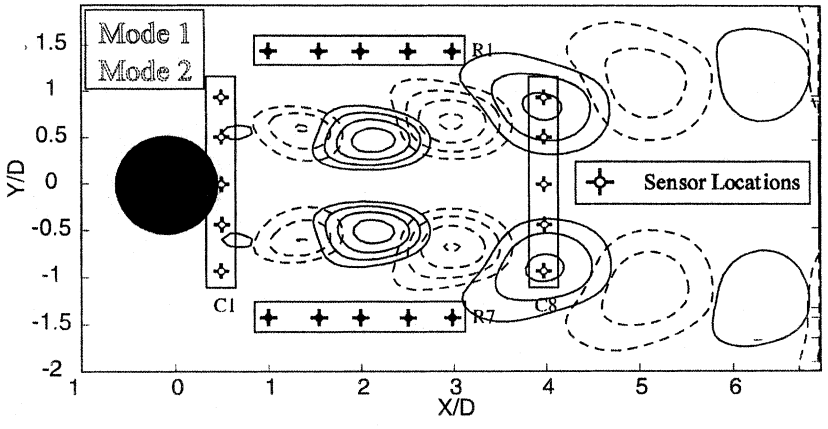

Figure 6. Column/row orientation (CFD data). Solid lines, magnitude of mode 1; dashed lines, magnitude of mode 2.

mode 1. The results reflect this preference in lower errors for mode 1. These examples introduced here highlight the benefit of using the heuristic approach for sensor placement and number with a quantitative measure of the performance. The heuristics quickly provide a relatively small number of potential candidates for sensor configurations. The selection of a configuration has to be based on a trade-off between the number of sensors and performance demands.

Based on the results presented in Table 2(a), the desired heuristics of sensor placement and number can be summarized as follows.

- Obtain the spatial distributions (modes) and the temporal coefficients of a POD model based on an adequate set of velocity snapshots.
- For the first four sensors, locate them at the maxima and minima of the modes closest to the cylinder. Locate the next set of sensors at the next maxima and minima, further away from the cylinder.
- Apply a quantitative criterion to assess the performance of each of the sensor configurations.
- The rationale behind the decision to select a specific sensor configuration should be based on a trade-off between performance and the cost of sensors.
- Finally, ensure that the controller design is robust for the estimation errors.

An important question to be addressed is whether POD based designs are robust. An insight into this question is obtained by comparing the POD based sensor configurations to 21 additional ad hoc designs. Further runs were conducted to search for a more conventional pattern for sensor placement. Consideration for the maxima and minima was not taken into account for the ad hoc approach. Three approaches were taken to search for a pattern that produced smaller error values. These five-sensor patterns included rows, columns, and arcs. Figures 6 and 7 show the configuration patterns.

The column approach began at X/D=0.5–4.0 at steps of 0.5. The five sensors were placed at Y/D positions of 1, 0.5, 0, –0.5, and –1. Eight column configurations were examined (see C1–C8 in Figure 6) and the CFD results are shown in Table 2(b).

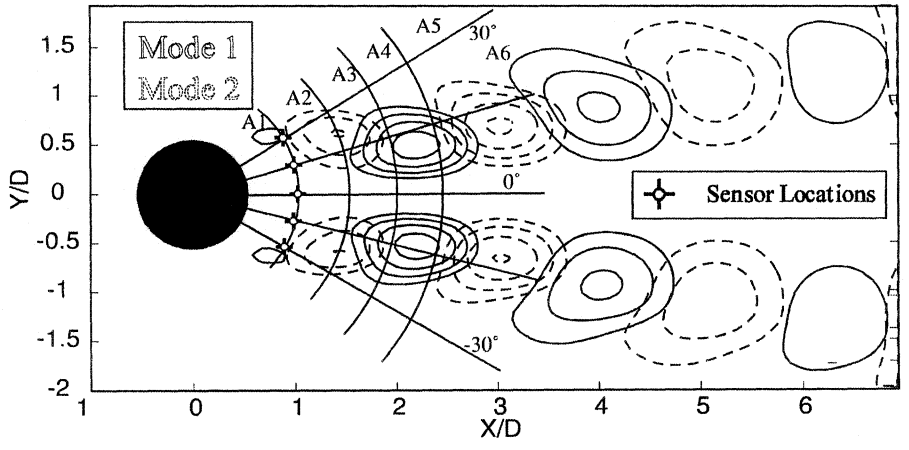

Figure 7. Arc orientation (CFD data). Solid lines, magnitude of mode 1; dashed lines, magnitude of mode 2.

The row approach was similar to the column approach and began at the *Y/D*=1.5 position and shifted down in increments of 0.5 diameters to the *Y/D* position of −1.5. The five sensors were placed at *X/D* positions of 1, 1.5, 2, 2.5, and 3. Seven row configurations were examined (see R1–R7 in Figure 6) and the CFD results are shown in Table 2(b).

In the arc approach, sensors were placed along arc segments at 30, 15, 0, −15, and −30 degrees from the centerline. The arcs were located 0.5 diameters off the surface of the cylinder (r = 1.0) and increased in radius by 0.5 diameters to a radius of 3.5 diameters from the center of the cylinder. Six arc configurations were examined (see A1–A6 in Figure 7) and the CFD results are shown in Table 2(b).

7. RESULTS OF AD HOC CONFIGURATIONS WITH CFD DATA

7.1. "Column" Configurations (CFD)

As seen in Figure 8, the error associated with the column configurations was small (less than 6%) for locations near the cylinder (C1–C4) and increased further downstream (C5–C8). The smallest mode 1 and mode 2 errors were 0.8% and 0.7%. The highest mode 1 and mode 2 errors were 26.7% and 53.6%. This probably corresponds to fluctuations being more intense nearer to the cylinder and decreasing downstream.

7.2. "Row" Configurations (CFD)

As seen in Figure 9, the row configurations above and below the centerline (R1–R3 and R5–R7) produced good results (less than 10% error for modes 1 and 2). Configuration R4, the five sensors downstream of the cylinder along the centerline, produced almost 100% error for both modes. This corresponds to the absence of mode 1 and mode 2 spatial eigenfunctions along the centerline.

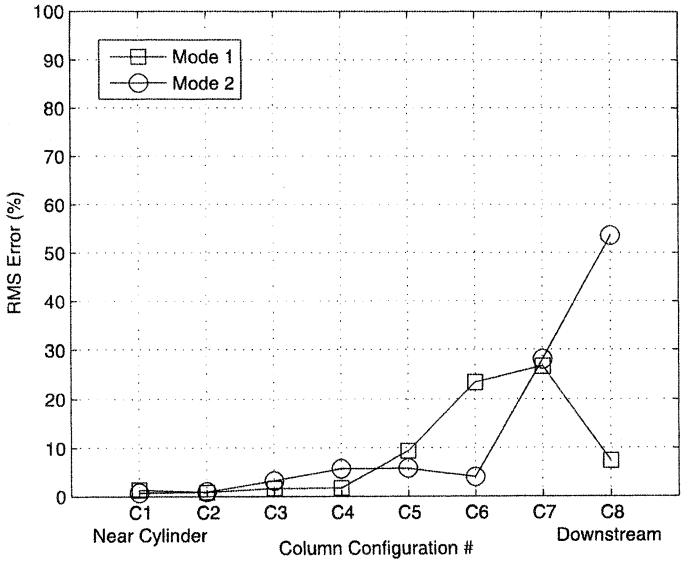

Figure 8. Column configuration error plot (CFD data).

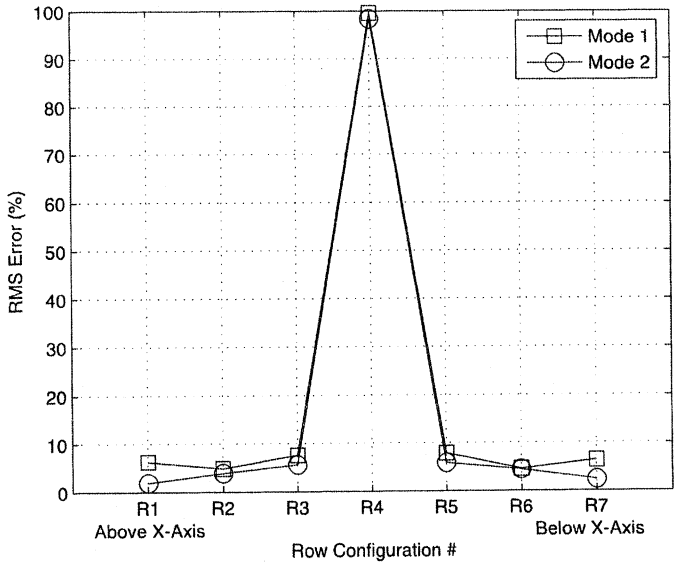

Figure 9. Row configuration error plot (CFD data).

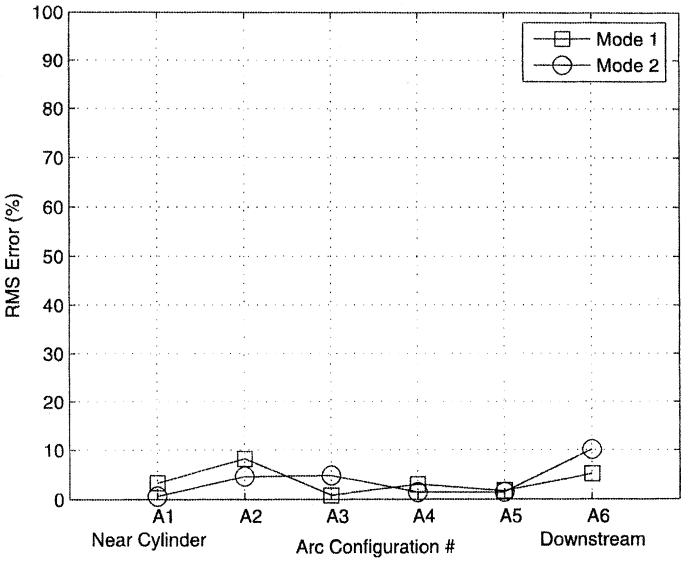

Figure 10. Arc configuration error plot (CFD data).

7.3. "Arc" Configurations (CFD)

As seen in Figure 10, the arc approach produced the most consistent error of all three ad hoc approaches. Both errors were at or below an rms value of 10%. Overall, the arc approach in designing senor locations and evaluating with CFD data seemed the best of the ad hoc approaches. Compared to the maxima/minima approach, the arc configurations resulted in similar small errors for modes 1 and 2 for CFD data. However, the different approaches must be validated with noisy experimental data to compare the robustness of the designs.

8. EXPERIMENTAL SETUP AND VALIDATION

The basis for validation of the design concerning sensor configuration was experimentally obtained velocity measurements in the wake of a circular cylinder at Re = 99. The experimental measurements were obtained in the Eidetic Model 2436 recirculating water tunnel. The water tunnel is situated in the Aeronautics Laboratory at the USAF Academy. The cross-section of the water tunnel is 38 × 38 cm^2 and the test section is 1.5 m in length. The circular cylinder model, as depicted in Figure 14, is comprised of a stainless steel rod, has a diameter, D, of 3.97 mm and a span, L, of 381 mm. The aspect ratio of the cylinder, L/D, is about 95. The cylinder was positioned horizontally in the water tunnel. The actuation system shown in Figure 15 was not used for the unforced experiments in this paper. Water tunnel velocity measurements were taken at three different Reynolds numbers, as detailed in Table 3.

The Reynolds number ($\mathrm{Re} = U_\infty D/\nu$) is calculated from the freestream velocity, U_∞, obtained from PIV velocity measurements. The kinematic viscosity, ν, is calculated on the

Table 3. Validation of the PIV data (Re versus St).

Reynolds number	Expected Strouhal number (Williamson, 1996)	Observed Strouhal number	Percent difference (%)
82	0.155	0.162	4.52
96	0.164	0.174	6.10
99	0.165	0.156	5.45

basis of temperature measurements. The natural shedding frequency of the cylinder, f, was calculated from the period of the time-dependent mode amplitude, a_1, as shown in Figure 4. The calculated Strouhal number ($\mathrm{St} = f\ D/U_\infty$) was then obtained based on the shedding frequency calculation. Williamson (1996) provides an equation based on experimental data that correlates the Reynolds number to the Strouhal number for a circular cylinder, and this information is used to calculate the expected Strouhal number. In Table 3, the expected and the calculated Strouhal numbers are compared. Furthermore, an uncertainty analysis provides a Reynolds number accuracy of ± 7.5 (or 6–7% error). The superposition of the percent difference presented in Table 3 on the data provided by Williamson (1996) validates the experimental Reynolds numbers of 82, 96, and 99.

The digital PIV system provided two-dimensional velocity field measurements in the wake of the cylinder. The field of view extended from the trailing edge of the cylinder to approximately eight diameters (8D) downstream. The PIV system employed a 1 Mpixel CCD camera (see Siegel et al., 2003). It was operated in dual exposure mode using cross-correlation to determine the pixel displacements based on two snapshots. A 32 × 32 pixel interrogation area with 50% overlap was used in the data reduction. This setup results in a vector field of 49 × 49 vectors. The field has a spatial resolution in the streamwise direction from –3.6 to 7.8 cylinder diameters. Each vector map was post-processed using a two-step sequence. First, a validation routine examined a 5 × 5 vector area and replaced rejected vectors with an averaged estimate. Secondly, an averaging filter was applied to each 5 × 5 vector area to reduce noise. To compensate for missing vectors, the software averaged the surrounding vectors and substituted a vector in its place.

9. RESULTS OF MAXIMA AND MINIMA CONFIGURATIONS WITH EXPERIMENTAL DATA

The experimental data were acquired at Reynolds numbers of 82, 96, and 99. For each case, 200 snapshots were acquired and a similar POD and estimation process, as undertaken with the CFD data, was repeated for each of the sensor configurations. The uncertainty of the PIV velocity measurements was estimated to be about 7–8% of the free stream velocity, based on the laser timing and displacement of the particles between snapshots. In Table 2(a), it can be seen that a five-sensor configuration, like configuration 8, reduces the rms of the estimation error to within 10%. This error should be acceptable for a moderately robust controller. For the velocity measurement error of 7–8%, it seems that beyond five sensors, the improvement in estimation error is relatively marginal.

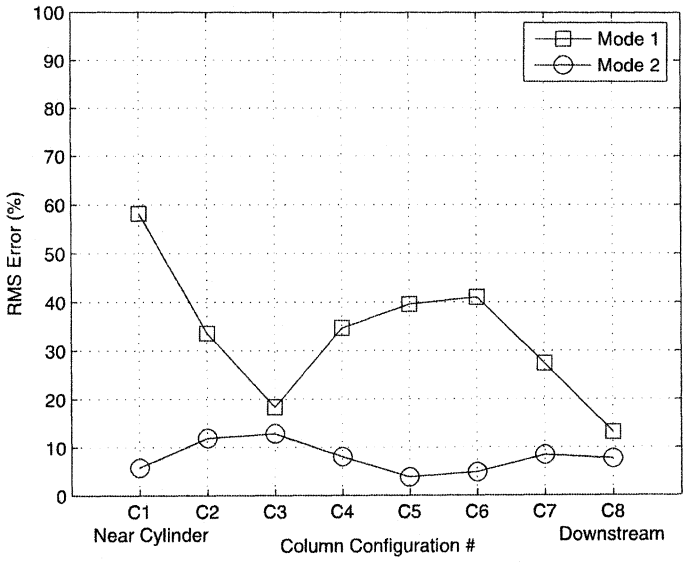

Figure 11. Column configuration error plot (experimental data).

10. RESULTS OF AD HOC CONFIGURATIONS WITH EXPERIMENTAL DATA

10.1."Column" Configurations (Experimental)

As seen in Figure 11, the experimental data produced worse results as compare to the CFD data. There is an overall increase in error. The mode 1 errors for all eight configurations are above 10% and the worst being 58.2%. Mode 2 error varies between 3.8% and 12.9%. There seems to be no correlation between error and proximity to the cylinder. There is little robustness with the column approach when validating the CFD data with experimental data.

10.2."Row" Configurations (Experimental)

As seen in Figure 12, the row error shows a trend of less error away from centerline similar to that of the CFD data. This approach, as validated by the experimental data, is somewhat robust, but not as robust as the maxima/minima approach.

10.3."Arc" Configurations (Experimental)

As seen in Figure 13, the experimental data produced worse results compared to the CFD data. There is an overall increase in error. The mode 1 errors for all eight configurations are above 10% and the worst being 44.5%. Mode 2 error varies between 3.5% and 14%. The arc approach has poor robustness when validated with experimental data, especially for mode 1.

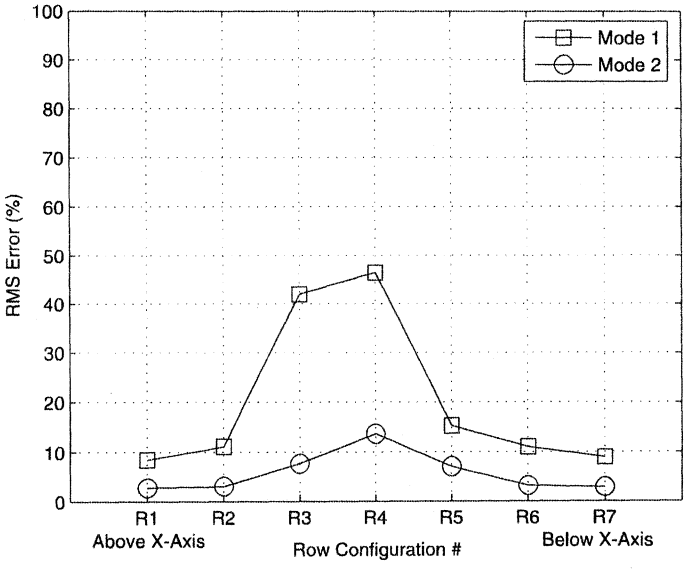

Figure 12. Row configuration error (experimental data).

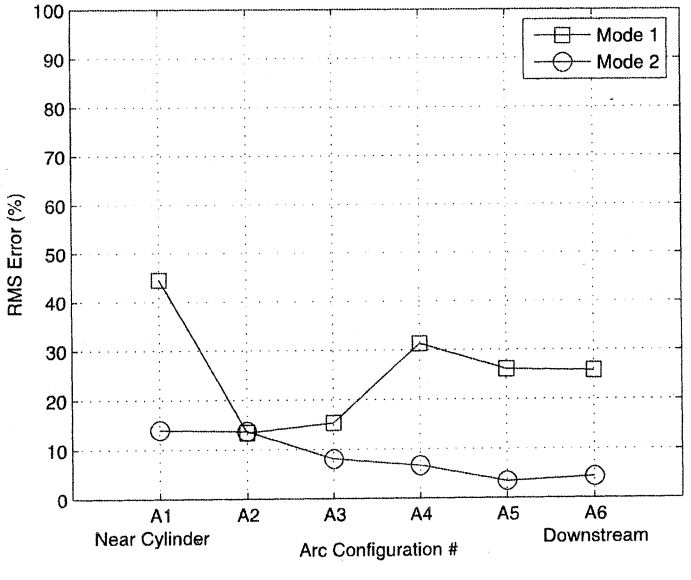

Figure 13. Arc configuration error (experimental data).

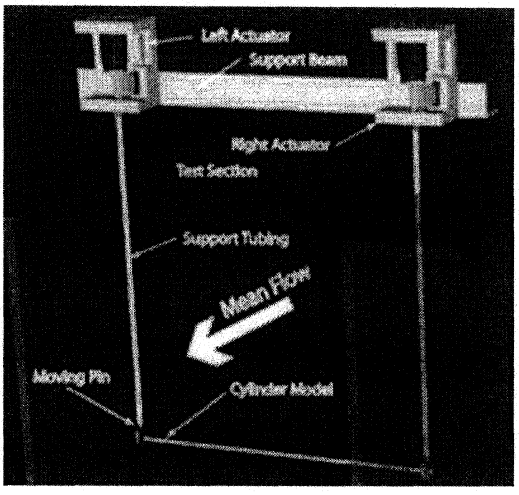

Figure 14. Experimental circular cylinder model.

Table 4. Gains lookup table for different Reynolds numbers for eight-sensor configuration 12. Superscipt "1" denotes CFD data and superscript "2" denotes water tunnel experimental data.

Mode 1 Reynolds number	C_{11}	C_{12}	C_{13}	C_{14}	C_{15}	C_{16}	C_{17}	C_{18}
100^1	0.9631	–0.0166	–0.5156	0.5386	–4.6397	4.6568	–3.2641	3.2496
82^2	0.3105	–0.1366	–0.2245	0.2099	–0.0408	0.0325	–0.0877	–0.0712
96^2	–0.6573	–0.3750	–0.3212	–0.5686	0.3732	–0.0449	0.8798	0.7341
99^2	–0.2235	0.2530	0.1961	–0.0961	0.2004	–0.2968	–0.0341	–0.0113
Mode 2 Reynolds number	C_{21}	C_{22}	C_{23}	C_{24}	C_{25}	C_{26}	C_{27}	C_{28}
100^1	–0.1500	0.7299	–1.8723	2.3083	4.3934	–5.4766	0.3387	–0.2640
82^2	0.2093	–0.0438	0.1294	–0.0001	0.1284	–0.1252	–0.5645	0.2556
96^2	0.3544	–0.6635	0.4564	–0.5365	0.1280	–0.1721	–0.5719	1.0155
99^2	0.0296	–0.2956	–0.0573	0.0226	0.1151	–0.1450	–0.2030	0.5293

All ad hoc designs had some useful configurations that resulted in an rms error below 10% with CFD data. However, these designs either had poor robustness when validated with experimental data or were less robust than the maxima/minima approach. The POD-based, maxima/minima, senor configuration design is better in that it is simple to implement and yields robust results between CFD design and experimental validation.

As mentioned earlier, the estimation scheme, based on the LSE procedure, predicts the temporal amplitudes of the first two POD modes from a finite set of measurements obtained

from CFD/experimental data. The coefficients C_s^n in equation (4) are obtained via the LSE method from the set of discrete snapshots (200 for experiments and 70 for CFD simulation) and temporal mode amplitudes and are presented in Table 4. This procedure is performed off-line just once for each Reynolds number. The main advantage of this approach is that it enables us to use sensors at fixed sensor locations with just the coefficients C_s^n adapting to the Reynolds number using the lookup table presented in Table 4. Basically, C_s^n represents the gains of the estimator and the lookup table is the gain scheduler based on the modal estimation provided by equation (4).

11. CONCLUSIONS AND RECOMMENDATIONS

A heuristic procedure was developed to determine the placement and number of sensors for the feedback control suppression of the wake instability behind a circular cylinder. This procedure is based on a low-dimensional, POD modeling and LSE. The development of the procedure was based on CFD simulations of a cylinder at a Reynolds number of 100. In all, 32 different sensor configurations were developed having between two and ten sensors. Experimental studies, based on noisy experimental data obtained from the water tunnel cylinder model at a Reynolds number of 99, validated the effectiveness of the developed sensor placement and design procedure. The results show that a five-sensor configuration can keep the rms estimation error, for the first two mode amplitudes, to within 10% in the case of noisy experimental measurements. This level of error is acceptable for a moderately robust controller. The performance improvement obtained by introducing additional sensors does not seem to justify the cost. The results show that the POD-based design is simple, effective and robust compared to ad hoc approaches.

Additionally, a gain-scheduling approach is proposed, whereby, for a given sensor configuration, the estimation and controller gains adapt by means of a lookup table to the variation in the Reynolds number, ranging from 82–100. This method is relatively simple and easy to implement in a real-time scenario.

Further research will aim at refining the developed heuristic procedure for sensor number and placement by taking into account symmetry, with respect to the x-axis. In this paper, we noticed the potential for estimation error improvement by placing sensors at locations that overlap "hillsides" of maxima/minima of modes 1 and 2. This potential should be further examined in a sensitivity study. Furthermore, there may be additional cost improvements to be gained by implementing a non-linear estimator instead of the linear stochastic estimator. It will be beneficial to examine the generic nature of the developed strategy for different bluff body geometries and Reynolds numbers. Finally, it would be important to compare the performance of the developed procedure with that obtained using an automated optimal search pattern.

REFERENCES

Abergel, F. and Temam, R., 1990, "On some control problems in fluid mechanics," *Theoretical and Computational Fluid Dynamics* **1**, 303–325.

Adrian, R. J., 1977, "On the role of conditional averages in turbulence theory," in *Proceedings of the 4th Biennial Symposium on Turbulence in Liquids*, Rolla, MO, J. Zakin and G. Patterson, eds., Science Press, Princeton, NJ, pp. 323–332.

Alhorn, B., Seto, M. L., and Noack, B. R., 2002, "On drag, Strouhal number and vortex-street structure," *Fluid Dynamics Research* **30** (6), 379–399.

Balas, M. J., 1978, "Active control of flexible systems," *Journal of Optimization Theory and Applications* **25** (3), 217–236.

Baruh, H. and Choe, K., 1990, "Sensor placement in structural control," *Journal of Guidance and Control* **13** (3), 524–533.

Blevins, R., 1990, *Flow Induced Vibration*, 2nd edition, Van Nostrand-Reinhold, New York.

Bonnet, J. P., Cole, D. R., Delville, J., Glauser, M. N., and Ukeiley, L. S., 1994, "Stochastic estimation and proper orthogonal decomposition: complementary techniques for identifying structure," *Experiments in Fluids* **17**, 307–314.

Carlson, H. and Miller, R., 2002, "Reduced-order modeling and sensing of flow separation on lifting surfaces," AIAA Paper 2002-0975.

Cohen, K., Siegel, S., McLaughlin, T., and Gillies, E., 2003a, "Feedback control of a cylinder wake low-dimensional model," *AIAA Journal* **41** (7), 1389–1391.

Cohen, K., Siegel, S., McLaughlin, T., and Myatt, J., 2003b, "Proper orthogonal decomposition modeling of a controlled Ginzburg–Landau cylinder wake model," AIAA Paper 2003-1292.

Deane, A. E., Kevrekidis, I. G., Karniadakis, G. E., and Orszag, S. A., 1991, "Low-dimensional models for complex geometry flows: Application to grooved channels and circular cylinders," *Physics of Fluids A* **3** (10), 2337–2354.

de Noyer, B., 1999, *Tail Buffet Alleviation of High-Performance Twin-Tail Aircraft Using Offset Piezoceramic Stack Actuators and Acceleration Feedback Control*, PhD Thesis, Aerospace Engineering, Georgia Institute of Technology, Atlanta, GA.

Gerhard, J., Pastoor, M., King, R., Noack, B. R., Dillmann, A., Morzynski, M., and Tadmor, G., 2003, "Model-based control of vortex shedding using low-dimensional Galerkin models," *AIAA Paper* 2003-4262.

Gillies, E. A., 1998, "Low-dimensional control of the circular cylinder wake," *Journal of Fluid Mechanics* **371**,157–178.

Holmes, P., Lumley, J. L., and Berkooz, G., 1996, *Turbulence, Coherent Structures, Dynamical Systems and Symmetry*, Cambridge University Press, Cambridge.

Li, Z., Navon, I. M., Hussaini, M. Y., and Le Dimet, F. X., 2003, "Optimal control of cylinder wakes via suction and blowing," *Computers and Fluids* **32**, 149–171.

Lim, K. B., 1997, "A disturbance rejection approach to actuator and sensor placement," NASA CR-201623.

Meirovitch, L., 1990, *Dynamics and Control of Structures*, Wiley, New York, pp. 313–351.

Min, C. and Choi, H., 1999, "Suboptimal feedback control of vortex shedding at low Reynolds numbers," *Journal of Fluid Mechanics* **401**, 123–156.

Oertel, H. Jr, 1990, "Wakes behind blunt bodies," *Annual Review of Fluid Mechanics* **22**, 539–564.

Panton, R. L., 1996, *Incompressible Flow*, 2nd edition, Wiley, New York, 384–400.

Park, D. S., Ladd, D. M., and Hendricks, E. W., 1993, "Feedback control of a global mode in spatially developing flows," *Physics Letters A* **182**, 244–248.

Roussopoulos, K., 1993, "Feedback control of vortex shedding at low Reynolds numbers," *Journal of Fluid Mechanics* **248**, 267–296.

Siegel, S., Cohen, K., McLaughlin, T., and Myatt, J., 2003, "Real-time particle image velocimetry for closed-loop flow control studies," AIAA Paper 2003-0920.

Siegel, S., Cohen, K., Smith, D., and McLaughlin, T, 2002, "Observability conditions for POD modes in a circular cylinder wake," in *Proceedings of the 55th APS/DFD Meeting*, Dallas, TX, Vol. 47, No. 10, Paper DN 4.

Sirovich, L., 1987, "Turbulence and the dynamics of coherent structures, Part I: Coherent structures," *Quarterly of Applied Mathematics* **45** (3), 561–571.

Smith, D. R., Siegel, S., and McLaughlin T., 2002, "Modeling of the wake behind a circular cylinder undergoing rotational oscillation," AIAA Paper 2002-3066.

von Kármán, T., 1954, *Aerodynamics: Selected Topics in Light of their Historic Development*, Cornell University Press, Ithaca, New York.

Williamson, C. H. K., 1996, "Vortex dynamics in the cylinder wake," *Annual Review of Fluid Mechanics* **28**, 477–539.